THE PUBLISHING HOUSE
OF THE ROMANIAN ACADEMY

PROCEEDINGS OF THE ROMANIAN ACADEMY, Series A,
Volume 20, Number 2/2019, pp. 131–138

ATTENUATION PHENOMENA IN GYROELECTRIC WAVEGUIDES WITH ANISOTROPIC DIELECTRIC LAYER

Darius PLONIS, Andrius KATKEVIČIUS, Vacius MALIŠAUSKAS

Vilnius Gediminas Technical University, Department of Electronic Systems, Vilnius, Lithuania
Corresponding author: Darius PLONIS, E-mail: darius.plonis@vgtu.lt

Abstract. Models of gyroelectric GaAs waveguides with temperature sensitive anisotropic dielectric layer are presented in this paper. The influence of density of free carriers and temperature to the EM waves attenuation of gyroelectric *n* and *p* GaAs waveguides is evaluated. Differential Maxwell's equations, coupled mode and partial area methods, coherent approaching, least square methods were used in order to obtain complex dispersion equations of models of gyroelectric waveguides with temperature sensitive anisotropic dielectric. The analysis of models of gyroelectric waveguides with temperature sensitive anisotropic dielectric shows that different effects and exceptions occur in *n*-GaAs and *p*-GaAs waveguides with external dielectric layers. Different effects and exceptions especially occur in cases, when were are relatively high density of impurities $N = 5 \cdot 10^{19}$ and $10^{20}\,\mathrm{m}^{-3}$ and limit temperatures $T = 125$ K as well as 200 K. The attenuation of electromagnetic waves is higher for *n*-GaAs compared with *p*-GaAs waveguides, because electrons are characterized by a lower effective mass and higher mobility in comparison with holes.

Key words: electromagnetic propagation, propagation constant, semiconductor waveguides, magnetic flux density.

1. INTRODUCTION

Dielectric waveguides are the partial case of gyroelectric waveguides. New models of dielectric waveguides consist of dielectric core and anisotropic dielectric layer. The anisotropic dielectric layer consists of silver and dielectric rings. These models of dielectric waveguides with anisotropic dielectric layer could be applied in the field of telecommunications, photonic transmission lines and nanowire waveguides [1,2].

Pousi and Lioubtchenko [3,4] have investigated waveguide antennas with dielectric rods. These antennas could be manufactured using GaAs semiconductor and monocrystalline Sapphire. Pousi and Lioubtchenko have discovered that these antennas can be used as a feed of the reflector type antennas. The return loss of antennas with dielectric rods was more than 25 dB in both cases, when waveguides with the GaAs or Sapphire material were used.

The GaAs semiconductor can be used for the manufacture of the radio frequency switches, which are designed for the micro-electro-mechanical systems. The analysis of switches, which are based on GaAs semiconductor, is performed by using CST Microwave studio® in wide frequency range from 0 to 40 GHz [5].

Nickelson et al. have investigated dependences of the cut-off frequencies of the magnetoactive *p*-Ge and *p*-Si plasma waveguides modes on the density of holes. These waveguides were investigated in wide frequency range from 20 GHz to 100 GHz. The density of holes was selected in the range from $10^{18}\,\mathrm{m}^{-3}$ to $10^{20}\,\mathrm{m}^{-3}$. However, the attenuation of electromagnetic waves was not investigated in these magnetoactive waveguides [6].

Kelebekler et al. have used the method of moment (MoM) for the analysis of cylindrical waveguides, which were loaded with plasma columns. Electrodynamical models of waveguides with plasma and without external dielectric layer were used in [7,8]. The comparative analysis of the complex dispersion curve of the surface wave mode has showed good agreement between methods of MoM, exact solution and quasistatic solution [8]. Liu et al. have analyzed circular conducting waveguides, which were filled with the gyroelectric

material. The analysis was done using dyadic Green's functions. However, the attenuation of the electromagnetic waves was not analyzed in this paper [9].

Ranajit Dey et al. have investigated a circular waveguide, which was loaded with the dual post discontinuity. The dyadic Green's function has been used in order to compute the scattered field in a circular waveguide. Results of the investigation have been compared with the Ansoft HFSS® software package [10].

The design and experimental results of a rectangular matched feed-illuminated offset parabolic reflector antenna are presented in [11]. Authors claim that rectangular matched feed effectively suppress the unwanted high cross-polarization introduced by the offset geometry in an offset parabolic reflector antenna. For satisfactory operation of a rectangular matched feed, it is necessary that the higher order mode TE_{11} should be added in proper amplitude.

Semiconductors, which are used in light-emitting devices in the field of mid-infrared opto-electronic applications, are described in [12]. Huawei Liang et al. have investigated the three-layer cylindrical waveguides, which consist of three arbitrary material mediums. Authors have extracted the mode conditions of the metal/dielectric-coated terahertz hollow waveguides using the derived eigenvalue equations of the TE, TM and hybrid modes. Authors claim that TE_{01} mode is very significant for the hollow waveguides in term of low loss in the range of terahertz wave [13].

New electrically and magnetically biased graphene-based cylindrical waveguides are investigated by the D. Correas-Serrano et al. Authors have presented the results of investigation, when the grapheme-based cylindrical waveguides parameters were controlled by changing voltage and magnetic field. The proposed models of waveguides could be used in reconfigurable dipole antennas [14]. Semiconductor waveguides have small dimensions and weights; therefore, they could be also used in phased array antennas.

Models of gyroelectric waveguides with temperature sensitive anisotropic dielectric layer are less investigated, but their control capabilities are significantly higher. Gyroelectric waveguides could be controlled by the magnetic field, temperature, infrared rays, visible light and γ-rays.

The aim of this paper is to investigate electromagnetic (EM) waves attenuation in models of gyroelectric *n* and *p* GaAs waveguides with temperature sensitive anisotropic dielectric layer and to ascertain how EM waves attenuation depends on density of free carriers and temperature in gyroelectric *n* and *p* GaAs waveguides.

Several methods were used for the computer study:

- the differential Maxwell's equations, coupled mode and partial area methods were used to obtain complex dispersion equation of gyroelectric waveguides with temperature sensitive anisotropic dielectric;
- the coherent approaching (iterative), least square methods were used for calculation of normalized central working frequency of models of gyroelectric waveguides and EM waves attenuation in these waveguides [15,16].

There were problems encountered in selection of material's of gyroelectric waveguides when investigating and applying gyroelectric waveguides. Gyroelectric cores are hard and brittle, therefore cores usually have the shape of cylindrical circular cross section rods. The gyroelectric waveguides with external dielectric layers can be applied in order to modify the electrodynamical properties and increase resistance of gyroelectric cores and to reduce EM wave attenuation.

2. MATERIALS AND METHODS

2.1. Electrodynamical Model

The basic electrodynamical model of open cylindrical gyroelectric waveguides (OCGWs) with temperature sensitive anisotropic dielectric layer is presented in cylindrical coordinate system in Figure 1. The electrodynamical model consists of three areas. The first area of the model is the gyroelectric core, which is characterized by the complex permittivity tensor $\underline{\underline{\varepsilon}}_r^s$ and permeability $\mu_r^s = 1$. The second area of the model is temperature sensitive anisotropic dielectric layer, which is also characterized by the complex

permittivity tensor $\underline{\underline{\varepsilon}}_{\mathrm{r}}^{\mathrm{ad}}$ and permeability $\mu_{\mathrm{r}}^{\mathrm{ad}}=1$. The third area of the model is air, which permittivity and permeability are $\varepsilon_{\mathrm{r}}^{\mathrm{a}}=\mu_{\mathrm{r}}^{\mathrm{a}}=1$.

Other parameters are: r^{s} is the radius of gyroelectric (semiconductor) core; d is the width of temperature sensitive anisotropic dielectric layer; R is the radius of temperature sensitive anisotropic dielectric layer and $\mathbf{B}_0$ is the vector of magnetic flux density.

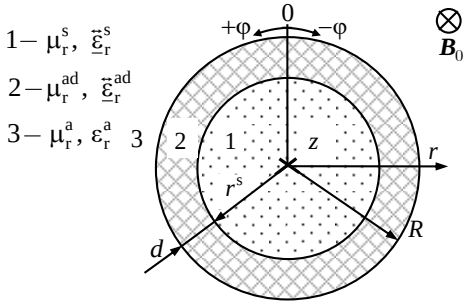

Fig. 1 – The basic electrodynamical model of open cylindrical gyroelectric waveguides with temperature sensitive anisotropic dielectric layer. The model consists of: 1 – gyroelectric core; 2 – temperature sensitive anisotropic dielectric layer; 3 – air [16].

The model of cylindrical gyroelectric waveguides is the electrodynamical system with distributed parameters. The previously mentioned parameters are not only structural OCGWs parameters of the model, but, most importantly, electrodynamical parameters.

2.2. The Simplified Mathematical Model of OCGWs

It's known, that gyroelectric core and anisotropic dielectric layer are characterized by complex permittivity tensors $\underline{\underline{\varepsilon}}_{\mathrm{r}}^{\mathrm{s}}$ and $\underline{\underline{\varepsilon}}_{\mathrm{r}}^{\mathrm{ad}}$. The complex tensor of gyroelectric core is calculated by the expression, which is presented in the monograph of L. Nickelson et al. [17].

The tensor of temperature sensitive anisotropic dielectric layer is calculated by using (Maxwell's-Garnet's) material mixing expressions [1,2]:

$$\underline{\underline{\varepsilon}}_{\mathrm{r}}^{\mathrm{ad}}(T)=\mathrm{diag}\left(\underline{\varepsilon}_{xx}(T),\ \underline{\varepsilon}_{xx}(T),\underline{\varepsilon}_{zz}(T)\right), \tag{1}$$

where $\underline{\varepsilon}_{xx}(T),\underline{\varepsilon}_{xx}(T),\underline{\varepsilon}_{zz}(T)$ are the diagonal elements of the complex tensor of temperature sensitive anisotropic dielectric layer. Complex elements of the tensor are presented below:

$$\underline{\varepsilon}_{xx}(T)=(1-N_d)\underline{\varepsilon}_{\mathrm{r}}^{\mathrm{d1}}+N_d\underline{\varepsilon}_{\mathrm{r}}^{\mathrm{d2}}(T);\quad \underline{\varepsilon}_{zz}(T)=\frac{\underline{\varepsilon}_{\mathrm{r}}^{\mathrm{d1}}\underline{\varepsilon}_{\mathrm{r}}^{\mathrm{d2}}(T)}{N_d\underline{\varepsilon}_{\mathrm{r}}^{\mathrm{d1}}+(1-N_d)\underline{\varepsilon}_{\mathrm{r}}^{\mathrm{d2}}(T)}, \tag{2}$$

where N_d is the filling ratio of permittivity $\underline{\varepsilon}_{\mathrm{r}}^{\mathrm{d2}}(T)$; $\underline{\varepsilon}_{\mathrm{r}}^{\mathrm{d1}}$ is the permittivity of the first TM-15 dielectric [17,18]; $\underline{\varepsilon}_{\mathrm{r}}^{\mathrm{d2}}(T)$ is the permittivity of the second dielectric, which is non-magnetic ferroelectric $Rb_{1-x}(ND_4)D_2PO_4$ material [19], which dielectric permittivity depends on the temperature T and frequency of EM waves.

Maxwell's equations, coupled mode and boundary conditions methods were used in order to receive the complex dispersion equation, which is 8th order complex determinant. The determinant of complex dispersion equation of OCGWs models with temperature sensitive anisotropic dielectric layer is presented in Figure 2. Here $\underline{a}_{jk}$ elements are the non-zero elements of determinant; j and k are the indexes of rows and columns, which indicate the $\underline{a}_{jk}$ place in the determinant.

The determinant consists of three parts. The first "g" part includes elements of determinant, which indicate the EM wave propagation in gyroelectric core. The second "ad" part includes elements of determinant, which indicate the EM wave propagation in temperature sensitive anisotropic dielectric layer. The last "a" part includes elements of determinant, which indicate the propagation of EM waves in the air.

Boundaries between the three areas are noted by the "g-ad" and "ad-a". The "g-ad" is the boundary between gyroelectric core and temperature sensitive anisotropic dielectric layer. The "ad-a" is the boundary

between temperature sensitive anisotropic dielectric layer and the air. Arrows correspond the same elements of the determinant.

g ad g-ad ad-a

$$\underline{D}^{\text{g-ad}} = \begin{vmatrix} \underline{a}_{11} & \underline{a}_{12} & \underline{a}_{13} & 0 & \underline{a}_{15} & 0 & 0 & 0 \\ \underline{a}_{21} & \underline{a}_{22} & 0 & \underline{a}_{24} & 0 & \underline{a}_{26} & 0 & 0 \\ \underline{a}_{31} & \underline{a}_{32} & \underline{a}_{33} & \underline{a}_{34} & \underline{a}_{35} & \underline{a}_{36} & 0 & 0 \\ \underline{a}_{41} & \underline{a}_{42} & \underline{a}_{43} & \underline{a}_{44} & \underline{a}_{45} & \underline{a}_{46} & 0 & 0 \\ 0 & 0 & \underline{a}_{53} & 0 & \underline{a}_{55} & 0 & \underline{a}_{57} & 0 \\ 0 & 0 & 0 & \underline{a}_{64} & 0 & \underline{a}_{66} & 0 & \underline{a}_{68} \\ 0 & 0 & \underline{a}_{73} & \underline{a}_{74} & \underline{a}_{75} & \underline{a}_{76} & \underline{a}_{77} & \underline{a}_{78} \\ 0 & 0 & \underline{a}_{83} & \underline{a}_{84} & \underline{a}_{85} & \underline{a}_{86} & \underline{a}_{87} & \underline{a}_{88} \end{vmatrix}$$

a

Fig. 2– The determinant of dispersion equation of models of open cylindrical gyroelectric waveguides with temperature sensitive anisotropic dielectric layer.

The $\underline{a}_{11}$, $\underline{a}_{12}$, $\underline{a}_{21}$, $\underline{a}_{22}$, $\underline{a}_{31}$, $\underline{a}_{32}$, $\underline{a}_{41}$, $\underline{a}_{42}$ and $\underline{a}_{57}$, $\underline{a}_{68}$, $\underline{a}_{77}$, $\underline{a}_{78}$, $\underline{a}_{87}$, $\underline{a}_{88}$ elements of determinant are presented in monograph [17]. Some non-zero elements of the second part of determinant are presented below:

$$\underline{a}_{13} = -\mathrm{J}_m(\underline{k}^{\text{da}}_{\perp 1} r^{\text{s}}); \quad \underline{a}_{15} = \mathrm{N}_m(\underline{k}^{\text{ad}}_{\perp 1} r^{\text{s}}), \tag{3}$$

$$\underline{a}_{44} = -\text{sign}\left(\frac{-\mathrm{j} m \mathrm{J}_m(\underline{k}^{\text{ad}}_{\perp 2} r^{\text{s}}) \underline{f}_{ad3}}{\underline{\Delta}_{ad} r^{\text{s}}} \right); \quad \underline{a}_{86} = \text{sign}\left(\frac{-\mathrm{j} m \mathrm{N}_m(\underline{k}^{\text{ad}}_{\perp 2} R) \underline{f}_{ad3}}{\underline{\Delta}_{ad} R} \right), \tag{4}$$

where $\mathrm{J}_m(\underline{k}^{\text{ad}}_{\perp 1,2} r^{\text{s}})$ is the Bessel function of the first kind of the *m*-th order with the complex argument $\underline{k}^{\text{ad}}_{\perp 1,2} r^{\text{s}}$; $\mathrm{N}_m(\underline{k}^{\text{ad}}_{\perp 1,2} r^{\text{s}})$ is the Bessel (Neumann) function of the second kind of the m-th order with the complex argument; $\underline{k}^{\text{ad}}_{\perp 1,2}$ are the transversal wave numbers in anisotropic dielectric layer; *m* is the first (azimuthal) index of the hybrid mode, which describes longitudinal wave constant component by the azimuthal perimeter coordinate φ; $\mathrm{j} = \sqrt{-1}$ is the complex number; f_{ad3} and $\underline{\Delta}_{ad}$ are the temporary coefficients and they can be calculated by the equations, which are presented below:

$$\underline{f}_{ad3} = \mathrm{j}\underline{\gamma}(k^2 \underline{\varepsilon}^{\text{ad}}_{xx} - \underline{\gamma}^2); \quad \underline{\Delta}_{ad} = k^4 \left(\underline{\varepsilon}^{\text{ad}}_{xx}\right)^2 - 2\underline{\gamma}^2 k^2 \underline{\varepsilon}^{\text{ad}}_{xx} + \underline{\gamma}^4, \tag{5}$$

where $\underline{\gamma} = \beta - \mathrm{j}\cdot\alpha$ is the complex propagation constant (here $\beta = \mathrm{Re}(\underline{\gamma}) = 2\pi/\lambda_w$ is the phase constant and λ_w is the wavelength of the waveguide modes; $\alpha = \mathrm{Im}(\underline{\gamma})$ is the attenuation constant); $k = \omega/c$ is the wave number in a vacuum.

Transversal wave numbers can be presented in anisotropic (isotropic) dielectric layer as [16]:

$$\underline{k}^{\text{ad}}_{\perp 1} = \sqrt{k^2 \underline{\varepsilon}^{\text{ad}}_{xx} - \underline{\gamma}^2}\ ; \quad \underline{k}^{\text{ad}}_{\perp 2} = \sqrt{\frac{\underline{\varepsilon}^{\text{ad}}_{zz}}{\underline{\varepsilon}^{\text{ad}}_{xx}} \left(k^2 \underline{\varepsilon}^{\text{ad}}_{xx} - \underline{\gamma}^2\right)}\ . \tag{6}$$

The external anisotropic dielectric layer transforms into isotropic layer, when filling ratio of permittivity becomes equal to $N_d = 1$. As the result the permittivity will become equal to $\underline{\varepsilon}^{\text{d2}}_{\text{r}}$. The external dielectric will have permittivity equal to $\underline{\varepsilon}^{\text{d1}}_{\text{r}}$, when the filling ratio of permittivity decreases to $N_d = 0$.

These waveguides can be transformed from one type to another type (1st type – gyroelectric core, anisotropic dielectric layer; 2nd type – gyroelectric core, isotropic dielectric layer; 3rd type – dielectric core (when $B_0 = 0$), anisotropic dielectric layer; 4th type – dielectric core, isotropic dielectric layer; 5th type – anisotropic dielectric tube (the permittivity of the core is equal to air); 6th type – isotropic dielectric tube).

The basic electrodynamical model of open cylindrical gyroelectric waveguides with temperature anisotropic dielectric layer can be used for analysis of different types of waveguides.

2.3. Permittivity of the external temperature sensitive anisotropic dielectric layer

Permittivity of the external temperature sensitive anisotropic dielectric layer consists of two dielectrics TM-15 and non-magnetic ferroelectric $Rb_{1-x}(ND_4)D_2PO_4$. As the authors claim in their researches [18] $Rb_{1-x}(ND_4)D_2PO_4$ dielectric has many advantages and has filled up the frequency gap between low frequencies and submillimeter waves. $Rb_{1-x}(ND_4)D_2PO_4$ dielectric can be used in wide temperatures range because the soft deuteron mode is polydispersive at all temperatures.

The permittivity of the real dielectric is complex when the electric field varies in the harmonic law. The real part of the permittivity is positive. It describes the possible polarization of the dielectric and is nonlinearly related to its absolute temperature (T, K) and frequency of the electric field (f, GHz) (Fig. 3a, 3c). The increase of real part of the permittivity is determined by the specific dielectric $Rb_{1-x}(ND_4)D_2PO_4$ material when the temperature increase. Consistent decline of the real part of permittivity with the steady increase of frequency is typical for all dielectrics. The imaginary part of the permittivity is negative. It describes losses in the dielectric and is non-linearly associated with the absolute temperature (T, K) and frequency of the electric field (f, GHz) (Fig. 3b, 3d). Polarization and thermal energy losses are possible in the dielectric. Polarization losses prevail in the low temperature T = 125 K range and are high in the low frequencies. Polarization losses decrease with the increase of the frequency. The opposite situation is with thermal losses. Thermal losses prevail over relatively high temperatures T = 200 K, are low in the low frequency range and grow with the increase of frequency. The maximum polarization and thermal losses are obtained in f = 20–30 GHz frequencies at the temperature T = 150 K.

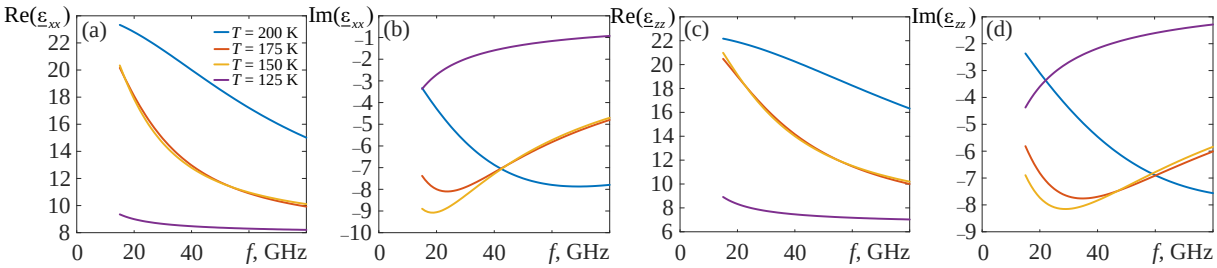

Fig. 3 – Dependencies of the anisotropic dielectric layer permittivity on the temperature and frequency: (a) – $\mathrm{Re}(\underline{\varepsilon}_{xx})$; (b) – $\mathrm{Im}(\underline{\varepsilon}_{xx})$; (c) – $\mathrm{Re}(\underline{\varepsilon}_{zz})$; (d) – $\mathrm{Im}(\underline{\varepsilon}_{zz})$, when the filling ratio of permittivity is N_d = 0.75.

Frequency characteristics of the real and imaginary parts of the permittivity are practically the same in the medium temperature range. The influence of temperature is negligible. The nature of the characteristics is similar in Fig. 3, but these figures have different frequency scales. This means that the relative dielectric permittivity in the direction of x and z axes is different, therefore, the used dielectric is anisotropic.

3. THE ANALYSIS OF ATTENUATION OF ELECTROMAGNETIC WAVES IN OCGWS

The analysis of OCGWs models was performed by taking into account density of electrons N, semiconductor mobility $\mu(T)$, effective mass m^*, temperature T and material type. $N = 10^{17}$; $5\cdot10^{18}$; $5\cdot10^{19}$; 10^{20} m^{-3} densities of electrons, T =125; 150; 175; 200 K temperatures, B_0 = 1 T magnetic flux density and d/r^s = 0.3 normalized width of external anisotropic dielectric layer were used in the investigation.

Waveguides of open cylindrical n-GaAs semiconductor were analyzed when the mobility of electrons have varied depending on the temperature μ(125 K) = 2.04 m^2/V·s; μ(150 K) =1.70 m^2/V·s; μ(175 K) = 1.46 m^2/V·s; μ(200 K) =1.28 m^2/V·s and effective mass was equal to $m^* = 0.067m_e$. A slightly different situation was encountered with waveguides, which were made from p-GaAs. The mobility of holes of these waveguides varied depending on the temperature μ(125 K) = 0.300 m^2/V·s; μ(150 K) = 0.197 m^2/V·s; μ(175 K) = 0.138 m^2/V·s; μ(200 K) =0.102 m^2/V·s when the effective mass was

equal to $m^* = 0.503m_e$. The dielectric constant of semiconductors was the same for both types of semiconductors and it was equal to $\varepsilon_r = 13.1$.

The density of impurities N has grown from 10^{17} m^{-3} to 10^{20} m^{-3} and has changed 1000 times in cores of waveguides. Nevertheless, this density of impurities was quite low in comparison with 10^{22}–10^{24} m^{-3} density of donors and acceptors impurities, which are applicable in monopolar and bipolar semiconductor devices. It was further observed that the temperature T has risen from 125 K (–148 ºC) to 200 K (–73 ºC) at a relatively narrow temperature range $\Delta T = 200 - 125 = 75$ K (ºC).

Electrodynamical parameters of models of open cylindrical GaAs semiconductor and semiconductor-dielectric waveguides with temperature sensitive anisotropic dielectric are presented in Table 1 (*n*-GaAs waveguides) and Table 2 (*p*-GaAs waveguides). Here $f_c r^s$ is the normalized central working frequency of the OCGWs and $\alpha_c r^s$ is the attenuation constant at central frequency. These parameters were received, when EM wave (mode) polarization is left-hand $\exp(+im\varphi)$, where m was the first azimuthal index of hybrid modes. m is equal to 1 in our calculations.

Table 1

The electrodynamical parameters of models of open cylindrical *n*-GaAs waveguides

N, m^{-3}	T, K	*n*-GaAs, $d/r^s = 0$		*n*-GaAs, $d/r^s = 0.3$	
		$f_c r^s$, GHz·m	$\alpha_c r^s$	$f_c r^s$, GHz·m	$\alpha_c r^s$
10^{17}	125	0.0412	0.0011	0.0339	0.0790
	150	0.0412	0.0010	0.0303	0.2211
	175	0.0412	0.0009	0.0303	0.2101
	200	0.0412	0.0008	0.0273	0.1161
$5\cdot10^{18}$	125	0.0412	0.0525	0.0338	0.1117
	150	0.0412	0.0480	0.0300	0.2441
	175	0.0412	0.0450	0.0300	0.2341
	200	0.0412	0.0420	0.0274	0.1371
$5\cdot10^{19}$	125	0.0408	0.5003	0.0346	0.1500
	150	0.0405	0.4812	0.0311	0.2211
	175	0.0405	0.4562	0.0311	0.4002
	200	0.0403	0.4312	0.0282	0.3272
10^{20}	125	0.0439	0.6833	0.0371	0.3992
	150	0.0430	0.6703	0.0329	0.4562
	175	0.0426	0.6483	0.0328	0.4113
	200	0.0420	0.4342	0.0292	0.4000

The attenuation coefficient α of EM waves at $d/r^s = 0$ has increased almost in direct proportion to the growth of density N of impurities and decreased with rising temperature T similarly for both *n*-GaAs and *p*-GaAs core types. The attenuation coefficient has increased about 48–53 times for *n*-GaAs core. The increase of attenuation coefficient have varied 38–55 times depending on the temperature T in a wider range for *p*-GaAs core, when the density of impurities has increased 50 times from 10^{17} m^{-3} up to $5\cdot10^{18}$ m^{-3}. The attenuation coefficient has increased approximately 10 times for *n*-GaAs core and 8–13 times for *p*-GaAs core depending on T when N became 10 times higher till $5\cdot10^{19}$ m^{-3}. The attenuation coefficient has increased more 1.4 times for *n*-GaAs core and about 2 times for *p*-GaAs core when the density of impurities increased 2 times from $N = 5\cdot10^{19}$ m^{-3} till 10^{20} m^{-3}.

The attenuation coefficient has increased about 540–720 times for *n*-GaAs core and 700–1090 times for *p*-GaAs core and that was about 1.3–1.5 times more as compared to 1000 times growth of density N of impurities from 10^{17} m^{-3} till 10^{20} m^{-3}.

The increase of normalized attenuation coefficient was logical and well understandable when the density of impurities and conductivity of semiconductors have increased but it was rather different for *n*-GaAs and *p*-GaAs. Normalized attenuation coefficient was always between 2 and 8 times higher for *n*-GaAs than *p*-GaAs because electrons are characterized by a lower effective mass and bigger mobility of electrons in comparison with holes. Therefore, cores with electronic conductivity of *n*-GaAs were used the most commonly.

Table 2

The electrodynamical parameters of models of open cylindrical *p*-GaAs waveguides

N, m^{-3}	T, K	*p*-GaAs, $d/r^s = 0$		*p*-GaAs, $d/r^s = 0.3$	
		$f_c r^s$, GHz·m	$\alpha_c r^s$	$f_c r^s$, GHz·m	$\alpha_c r^s$
10^{17}	125	0.0409	0.0003	0.0348	0.0743
	150	0.0409	0.0003	0.0310	0.2116
	175	0.0409	0.0002	0.0310	0.2115
	200	0.0409	0.0001	0.0278	0.1100
$5\cdot10^{18}$	125	0.0409	0.0125	0.0348	0.1300
	150	0.0409	0.0125	0.0310	0.2510
	175	0.0409	0.0075	0.0310	0.2349
	200	0.0409	0.0055	0.0278	0.1312
$5\cdot10^{19}$	125	0.0409	0.1578	0.0348	0.2056
	150	0.0409	0.1046	0.0310	0.2904
	175	0.0409	0.0735	0.0310	0.2581
	200	0.0409	0.0543	0.0278	0.1523
10^{20}	125	0.0416	0.3177	0.0353	0.3422
	150	0.4120	0.2099	0.0315	0.3587
	175	0.4120	0.1473	0.0315	0.3062
	200	0.4120	0.1085	0.0281	0.1868

The mobility of carriers have decreased in the low temperature area when density of impurities increased. The mobility increased $\mu_{n,p} \sim T^{3/2}$ in doped semiconductors as temperature raised. Presumably, all impurities regardless of their density were ionized at least in 125 K temperature in the cores of tested semiconductors. Attenuation coefficient has decreased due to chaotic crystal lattice and mobility of charge carrier by debilitating their relations with EM waves. Meanwhile normalized attenuation coefficient $\alpha_c r^s$ has increased in most cases, when cores of *n*-GaAs, *p*-GaAs were covered with external dielectric layer, which normalized thickness was equal to $d/r^s = 0.3$. This can be explained by the fact that the external anisotropic temperature sensitive dielectric layer has distracted the electromagnetic waves from the middle of semiconductor core and redistributed them on both sides of the border with the dielectric core. Therefore, the connection was reduced between carriers and waves, which were in the middle of the core and the main interaction of carriers and waves took place in the surface of the core. In addition to, attenuation of waves took places in the exterior layer because of losses in dielectric. However, this was carried out differently depending on the material of semiconductor, density of impurities and temperature.

The absolute values of attenuation coefficient have increased in *n*-GaAs and *p*-GaAs waveguides when density of impurities increased, because cores became more conductive and EM waves propagated in their thinner surface layer in most cases.

The relative increase, which was obtained as a $\alpha_c r^s$ ratio of the absolute values, has decreased, when the density of impurities increased: 1) when $N = 10^{17}$ m^{-3} the attenuation coefficient increased from 71.8 till 233 times for *n*-GaAs and from 248 till 1100 times for *p*-GaAs; 2) when $N = 5\cdot10^{18}$ m^{-3} – from 2.1 till 5.2 times for *n*-GaAs and from 10.4 till 31.3 for *p*-GaAs; 3) when $N = 5\cdot10^{19}$ m^{-3} – from 0.3 till 0.9 times for *n*-GaAs and from 1.3 till 3.5 times for *p*-GaAs; 4) when $N = 10^{20}$ m^{-3} – from 0.6 till 0.9 times for *n*-GaAs and from 1.1 till 2.1 times for *p*-GaAs.

4. CONCLUSION

The attenuation coefficient of the EM waves increases because of the influence of external anisotropic temperature sensitive dielectric layer. The attenuation coefficient increases by 2.2 times more in the *n*-GaAs waveguides compared with the *p*-GaAs waveguides. The attenuation coefficient decreases more in *p*-GaAs waveguides in comparison of attenuation coefficient in the *n*-GaAs cores, when $N = 5\cdot10^{19}$ and 10^{20} m^{-3}.

The attenuation coefficient $\alpha_c r^s$ increases from the lowest ($\alpha_c r^s = 0.0743$ – *p*-GaAs waveguides with external anisotropic layer) values at $T = 125$ K till the maximum ($\alpha_c r^s = 0.4562$ – *p*-GaAs waveguides with

external anisotropic layer) value at T = 150 K or less frequent at T = 175 K in *n*-GaAs and *p*-GaAs waveguides in most cases.

The attenuation coefficient decreases to an intermediate ($\alpha_c r^s = 0.1868$ – *p*-GaAs) value between the minimum ($\alpha_c r^s = 0.1100$ – *p*-GaAs) and maximum ($\alpha_c r^s = 0.4000$ – *n*-GaAs) values, when the temperature rises up to 200 K, when the external anisotropic dielectric layer is used.

Different effects and exceptions occur in *n*-GaAs and *p*-GaAs waveguides with these cores and exterior dielectric layers especially in cases when there are relatively high density of impurities $N = 5 \cdot 10^{19}$ and 10^{20} m^{-3} and limit temperatures T = 125 K as well as 200 K. Their interpretations and applications are rather complicated and require more researches.

REFERENCES

1. Y.J. HUANG, W.T. LU, S. SRIDHAR, *Nanowire waveguide made from extremely anisotropic metamaterials*, Physical Review A, **77**, *6*, pp. 1–11, 2008.
2. Q. ZHANG, T. JIANG, Y. FENG, *Slow wave propagation in a dielectric cylindrical waveguide with anisotropic metamaterial cladding*, Microwave Conference APMC 2009, Asia Pacific, 2009, pp. 1242–1245.
3. J.P. POUSI, D.V. LIOUBTCHENKO, S.N. DUDOROV, J.A. MALLAT, A.V. RÄISÄNEN, *High permittivity dielectric rod waveguide antenna for 110–150 GHz*, 2006 First European Conference on Antennas and Propagation, Nice, 2006, pp. 1–4.
4. D.V. LIOUBTCHENKO, S.N. DUDOROV, J.A. MALLAT, A.V. RÄISÄNEN, *Dielectric rod waveguide antenna for W band with good input match*, IEEE Microwave and Wireless Components Letters, **15**, pp. 4–6, 2005.
5. S. CHATURVEDI, G.S. SARAVANAN, M.K. BHAT, S. BHALKE, S.L. BADNIKAR, R. MURALIDHARAN, S.K. KOUL, *Design and electrical characterization of waferlevel micro-package for GaAs-based RFMEMS switches*, IETE Journal of Research, **59**, *3*, pp. 201–209, 2013.
6. L. NICKELSON, S. ASMONTAS, V. MALISAUSKAS, R. MARTAVICIUS, *The dependence of open cylindrical magnetoactive p-Ge and p-Si plasma waveguide mode cutoff frequencies on hole concentrations*, J. Plasma Physics, **75**, *1*, pp. 35–51, 2008.
7. E. KELEBEKLER, N. YENER, *Backward wave modes of partially plasma column loaded cylindrical waveguide*, Progress In Electromagnetics Research Symposium Proceedings, Marrakesh, Morocco, Mar. 20–23, 2011, pp. 1084–1088.
8. E. KELEBEKLER, *Complex surface wave modes of plasma column loaded closed cylindrical waveguide*, Progress in Electromagnetics Research B, **54**, pp. 357–383, 2013.
9. S. LIU, L.W. LI, M.S. LEONG, T.S. YEO, *Theory of gyroelectric waveguides*, Progress in Electromagnetics Research, **29**, pp. 231–259, 2000.
10. R. DEY, S.B. CHAKRABARTY, R. JYOTI, T. KURIAN, *Higher order mode analysis of dual-post discontinuity in a circular waveguide*, IETE Journal of Research, **62**, *1*, pp. 55–62, 2015.
11. D. PUJARA, S.B. CHAKRABARTY, *Cancellation of high cross-polarization of an offset parabolic reflector antenna using a rectangular matched feed*, IETE Journal of Research, **58**, *4*, pp. 317–321, 2012.
12. S. MUKHERJEE Z. SHI, *State-of-the-art IV-VI semiconductor light-emitting devices in mid-infrared opto-electronic applications*, IETE Technical Review, **26**, *4*, pp. 236–246, 2009.
13. H. LIANG, S. RUANA, M. ZHANGA, H. SU, X. ZHAOA, *Mode theory of three-layer cylindrical waveguides and its application to aurum(Au) / polystyrene (PS) - coated terahertz hollow waveguides*, Optik, **125**, *13*, pp. 3076–3080, 2014.
14. D.C. SERRANO, J.S. GOMEZ-DIAZ, A. ALU, A.A. MELCÓN, *Electrically and magnetically biased graphene-based cylindrical waveguides: analysis and applications as reconfigurable antennas*, IEEE Transactions on Tetrahertz Science and Technology, **5**, *6*, pp. 951–960, 2015.
15. D. PLONIS, V. MALISAUSKAS, A. SERACKIS, *Semi-automatic analysis of gyrotropic semiconductor waveguides using neural network*, Acta Physica Polonica A, **119**, *4*, pp. 542–547, 2011.
16. D. PLONIS, A. KATKEVIČIUS, V. MALIŠAUSKAS, A. SERACKIS, D. MATUZEVIČIUS, *Investigation of new algorithms for estimation of losses in microwave devices based on a waveguide or a meander line*, Acta Physica Polonica A, **129**, *3*, pp. 414–424, 2016.
17. L. NICKELSON, S. ASMONTAS, V. MALISAUSKAS, V. SUGUROVAS, *The open cylindrical gyrotropic waveguides*, Technika, 2007.
18. V.I. WOLMAN, *Reference book of the calculation and design of microwave strip devices*, Moscow: Radio and Communication 1982. (original in Russian: Справочник по расчету и конструированию СВЧ полосковых устройств. Под ред. В. И. Вольмана. Москва: Радио и связь, 1982. – 328 с.).
19. J. BANYS, A. KAJOKAS, S. LAPINSKAS, A. BRILINGAS, J. GRIGAS, J. PETZELT, S. KAMBA, *Microwave and millimetre-wave dielectric response of Rb1–x(ND4)D2PO4 dipolar glass*, Journal of Physics-Condensed Matter, **14**, pp. 3725–3733, 2002.

Received March 15, 2017